RSC Advances

PAPER

View Article Online
View Journal | View Issue

Cite this: *RSC Adv.*, 2019, **9**, 30448

Synthesis and photovoltaic application of NIR-emitting perylene-monoimide dyes with large Stokes-shift†

Vikas Sharma, ‡[a] Kovida, ‡[a] Dhananjaya Sahoo,[a] Nonu Varghese,[b] Kallol Mohanta *[b] and Apurba Lal Koner *[a]

Received 26th June 2019
Accepted 18th September 2019

DOI: 10.1039/c9ra04833b

rsc.li/rsc-advances

An efficient Sonogashira coupling protocol is developed for tetra-alkynylation at the *bay* and *peri*-positions of the perylene-monoimide (PMI) dye in its PMI(Br)$_4$ form. The absorption band for these PMI dyes covered from the visible to Near-infrared (NIR) region and PMI(NMe$_2$)$_4$ is found to exhibit a record-breaking Stokes-shifted NIR emission with good photovoltaic properties.

Near-infrared (NIR) absorbing dyes are gaining a great deal of attention both in research and technology because of their widespread applications in diverse areas of bio-imaging, photothermal therapy, NIR triggered drug release and advanced optoelectronics.[3,4] NIR dyes are crucial for solar cell applications since the NIR region of the solar spectrum comprises almost 45% of the total energy transferred to the Earth through sunlight.[5] The theoretical calculation also showed significant augmentation in output power of solar cells fabricated using NIR absorbing materials.[6,7] Considering this, NIR dyes have attracted appreciable attention for their solar cell applications.[8] Most efficient NIR dyes follow the widespread D–π–A (D = Donor, π = conjugated bridge, A = Acceptor) framework for tuning ground and exited-state potentials.[3] This class of dyes is popularly known as intramolecular charge transfer (ICT) dyes, and they rely on strong donors to destabilize the ground-state potentials and acceptors to stabilize the exited-state potentials. This can be achieved either by extending the conjugation length or by covalently linking suitable donor–acceptor moiety with a π-bridge.[3]

Rylene based dyes are highly π-conjugated polyaromatic hydrocarbon (PAH) with outstanding chemical, thermal and photochemical stability.[9,10] Among the rylene dyes, perylene-monoimides (PMIs) are found to be suitable with more number of available positions (*i.e.*, *ortho*, *bay* and *peri*-) for chemical functionalization. Additionally, their strong optical absorptions can be tuned from visible to NIR regions by judicious modification.[11–13] This class of dyes has shown a wide range of applications in organic photovoltaics,[14] solar cells, dye lasers, optical sensors, photosensitizers,[15] optical memory device,[12] and bio-labels.[16] In this regard, tetra-brominated PMI is considered a versatile starting material for the synthetic modification at both *bay* and *peri* positions.[17,18] The extension of π-conjugation along *peri*-positions has a strong impact on the photophysical properties due to energetic optical transition (S_0–S_1).[17,19–21] The extension of π-conjugation along *bay*-positions can be used for fine-tuning of their optical properties.[22]

Effect of π-conjugation along one of the *peri*-position of PMI through ethynylene linker (Fig. 1) has been extensively studied to impact on optical properties.[23,24] Imahor group has expanded the perylene core through π-conjugation along two *bay* (1,6-) and one *peri* (9-)position *via* ethynylene linker between perylene core and triarylamine.[15] However expanding the PMI core through π-conjugation along both *peri* and *bay*-positions is still unexplored due to the limited access to the key building block, *i.e.*, PMI(Br)$_4$. Fortunately, our recent report on an elegant

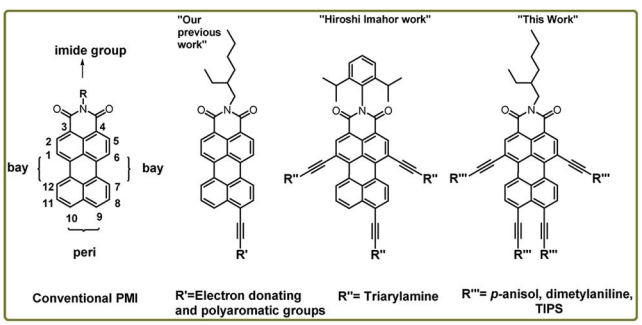

Fig. 1 Structure and functionalization possibility of PMI derivatives and NIR-emitting tetra-coupled PMI.

[a]Department of Chemistry, Indian Institute of Science Education and Research Bhopal, Bhopal Bypass Road, Bhauri, Bhopal, Madhya Pradesh, India. E-mail: akoner@iiserb.ac.in

[b]Department of Physics, PSG College of Technology & PSG Institute of Advanced Studies, Peelamedu, Avinashi Road, Coimbatore, 641004, Tamilnadu, India. E-mail: kma@psgias.ac.in

† Electronic supplementary information (ESI) available: Synthesis, all characterizations ^{1}H, ^{13}C, mass, IR, UV-Vis., emission, and photovoltaic experiments. CCDC 1911385. For ESI and crystallographic data in CIF or other electronic format see DOI: 10.1039/c9ra04833b

‡ These authors contributed equally.

method for the synthesis of PMI$(Br)_4$ allowed the desirable tetra-alkynylation of PMI in both *bay* and *peri*-position.[18]

In this work, the synthetic protocol for expanding the π-conjugation along both *bay* and *peri*-positions is demonstrated using fourfold Sonogashira cross-coupling reaction. Later, the effect of tetra-alkynylation on electronic, photophysical and redox properties is extensively investigated. Furthermore, the photovoltaic applicability has been studied to establish the prominent significance of the NIR-emitting PMI-derivatives.

To exploit this work, we have synthesized compounds **2a–c** by Sonogashira coupling reaction using different donor substituents at *bay* and *peri*-positions of the perylene core (Scheme 1). The synthesis commenced with the treatment of compound **1** with 4-ethynylanisole as the donor group in toluene : TEA (1 : 1) at 80 °C for 18 h using $Pd_2(dba)_3$ and P(*o*-tolyl)$_3$ as the catalyst and ligand respectively. This afforded the compound **2b** in 10% yield, and the same protocol was utilized to synthesize **2a**, but the reaction was unsuccessful. This prompted us to optimize the reaction conditions and thus compound **2a** was synthesized in 45% yield by coupling 4-ethynyl-*N*,*N*-dimethyl aniline with compound **1** in THF : DIPEA (1 : 1) at 80 °C for 18 h using tetrakis(triphenylphosphine) palladium (0) and CuI as the catalyst and co-catalyst respectively. The same approach failed to yield the compound **2b** by using 4-ethynylanisole as the alkyne linker while keeping other reaction conditions same. Unfortunately, a mixture of isomers was obtained, which were difficult to isolate through column chromatography. For the synthesis of compounds **2b** and **2c**, further modification was carried out by employing a different palladium-based catalyst *i.e.*, $PdCl_2(PPh_3)_2$. The reaction was performed *via* the treatment of compound **1** with 4-ethynylanisole in THF : TEA (1 : 1) at 80 °C for 18 h with $PdCl_2(PPh_3)_2$ and CuI as the catalyst and co-catalyst respectively. The residue was purified using column chromatography using DCM : Hexane (1 : 1) as the eluent and silica gel as the stationary phase. By following the optimized protocol compound **2b–c** were isolated in 60% and 71% yields respectively. This protocol involving the catalyst $PdCl_2(PPh_3)_2$ was also tested to synthesize the compound **2a** but the yield of the reaction was only 15%. Further, all the compounds **2a–c** were characterized by NMR and HRMS.

Single crystals of **2c** are grown by slow diffusion of methanol into a solution of the compound **2c** in hexane. The molecules are packed in the triclinic space group $P\bar{1}$ (for details see ESI†). In the crystal structure (see Fig. 2a), the bond angle between C≡C of the two TIPS groups attached at both *peri*-positions of PMI is distorted to an angle of 10–11° from 180° due to the steric congestion between bulky TIPS groups. Additionally, there is a twist of 16° in the perylene core due to TIPS groups at *bay* positions (Fig. 2b).

The synthesized PMI derivatives, **2a**, **2b**, and **2c** appear green, violet and pink respectively, in the solution phase with large absorption coefficients in the range of 10^6 M^{-1} cm^{-1} (see Fig. 3a). As is clear from the UV-Vis spectra, these compounds exhibit a broad absorption band covering most of the visible region and some part of NIR region which is a unique characteristic of a push–pull type PMI-based chromophore. The UV-Vis spectra of the tetra-coupled PMI (**2a–c**) in $CHCl_3$ showed their longest maxima at 665, 614 and 575 nm respectively and were bathochromically shifted by 65–150 nm with respect to the unsubstituted PMI with an absorption maximum at around 510 nm. It should be noted that for push–pull PMIs, orbital partitioning plays a very important role.[18] The orbital partitioning occurs when the HOMO coefficients on the donor part and the LUMO coefficient on the acceptor part in the same molecule are high. Here, in these molecules, this broad absorption in the visible region can be attributed to the orbital partitioning arising from the introduction of strong electron-donating substituents like –NMe_2, –MeO and TIPS at the *bay* and *peri* positions of the perylene core. Notably, the significant red-shifted absorption in PMI-$(NMe_2)_4$ can also be justified by the presence of lone pairs on nitrogen atoms which effectively enhances the conjugation length of the π-system in the molecule. Therefore, a drastic bathochromic shift can be achieved by suitable functionalization of the PMI core with strong electron donating groups.

The normalized fluorescence spectra of compounds **2a–c** in $CHCl_3$ are shown in Fig. 3b. From the emission characteristics of the derivatives, it can be ascertained that a significant red-shifted emission maximum by 30–210 nm are observed for all the derivatives. Notably, compound PMI-$(NMe_2)_4$ **2a** is found to have the broadest emission overlapping with the whole visible region and a significant part of NIR with a shoulder end at

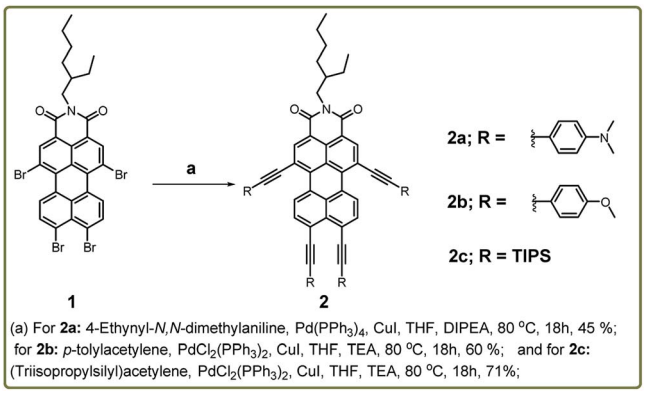

Scheme 1 Synthetic protocol for the preparation of tetra-coupled PMI derivatives **2a–c**.

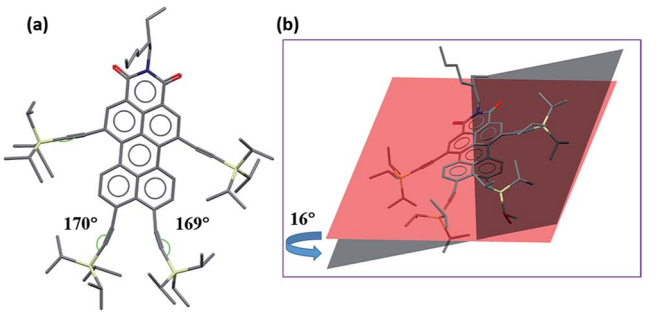

Fig. 2 Single crystal X-ray structure of compound **2c** (a) front view (b) side view to show the twisting in the perylene core.

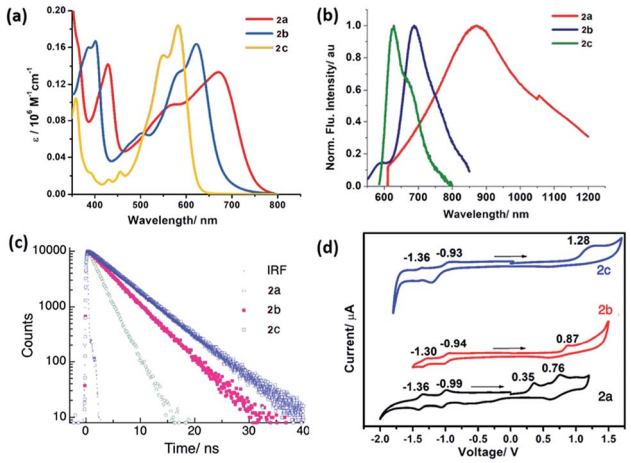

Fig. 3 (a) UV-Vis absorption spectra (5 μM) of the PMI derivatives in $CHCl_3$ (b) normalized emission spectra (5 μM) in $CHCl_3$ (C) fluorescence lifetime decay plot for the PMI derivatives in toluene and (d) cyclic voltammograms of the compounds in DCM (electrolyte: 0.1 M *n*-Bu_4NPF_6, ferrocene as the internal), arrows show the direction of CV scan.

1200 nm. This compound shows the emission maxima at 869 nm thus displaying a large Stokes shift of 204 nm as compared to methoxy and TIPS substituted analogs **2b** and **2c** (30–45 nm) with emission maxima at 660 nm and 606 nm respectively.

These low energy bands in these spectra are a characteristic of a strong emission from a charge transfer absorption arising from the electron donating groups present at *bay* and *peri*-positions to the electron accepting imide group through the π-conjugated system. PMI based ICT dyes are sensitive to the chemical environment, and consequently, their optical properties are highly-dependent on concentration, solvent polarity, and temperature. To check the effect of solvent polarity on the optical properties of these derivatives, the solvent-dependent absorption and emission spectra for all the compounds in various solvents are measured at 298 K (See Fig. S2–4, S6–8, and S10–12†). The fluorescence maxima are largely red-shifted in case of **2b** and **2c** while no significant change was observed in the absorption maxima under the same conditions indicating an increase in the dipole moment of the excited state compared to the ground state (see ESI†).[25,26] For example, for compounds **2b** and **2c**, a red shift in the emission maxima by *ca.* 40 nm and 20 nm respectively was observed while going from least polar to the most polar solvent. We obtained a linear correlation between Stokes-shift and solvent polarity parameter (E_T(N), Fig. S13†). The large Stokes-shift in case of **2a** may also be due to the intramolecular twisting.[15,27] Such intramolecular twisting should be significant enough to cause a shift in the emission and not too large to destroy the conjugation and planarity. Further, the fluorescence lifetime of the compounds **2a–c** was found to be 2.1, 4.3 and 5.5 ns in toluene (Fig. 3c). The electrochemical properties of these dyes were investigated by cyclic voltammetry in CH_2Cl_2 solution containing 0.1 M *n*-Bu_4NPF_6 as the supporting electrolyte and ferrocene as the internal standard. The obtained redox potentials and the calculated values for the HOMO–LUMO energy levels are summarized in Table 1. The oxidation potentials of these tetra-coupled PMIs are highly dependent on the electron donating abilities of the attached substituents. The analysis of HOMO energy levels shows that as the electron donating ability of the attached donor is increasing, the HOMO energy level is becoming more positive as evident from −5.93 eV for **2c** and −5.76 eV for **2b** to −5.54 eV for **2a** (Fig. 3d). The CV curve for compound **2a** shows two reversible oxidation waves at E_{ox} values of 0.35–0.76 V and two reversible reduction waves at E_{red} values of −0.99 to −1.36 V, which indicates the formation of radical cations by oxidation and radical anions upon reduction. Contrary to this, curve for compound **2b** undergoes one quasi-reversible oxidation at E_{ox} value of 0.87 V and two reversible reductions at E_{red} values of −0.94 to −1.30 V. This can be attributed to the replacement of –NMe_2 group with –OMe leading to the shift in the value to the positive direction for reduction as well as oxidation. Compound **2c** on the other hand shows one oxidation wave at E_{ox} value of 1.28 V and two reversible waves at E_{red} values of −0.93 to −1.36 V. One interesting feature observed in these calculations was that depending on the substitution at *peri* and bay-positions the onset potentials can be easily tuned with significant values. This observation was further validated using DFT calculations which were performed using B3LYP as functional and DNP as the basis set. The optimized FMO of **2a** and **2b** are depicted in Fig. S14 and 15.† Furthermore, as expected the HOMO potential on varying the substituents at *peri* position were in good agreement with the data obtained from the electrochemical and optical measurements. Also, from the theoretical and experimental data, it was observed that there was a marked reduction in the band gap values for these compounds concerning the unsubstituted PMI.

We tried to see the applicability of the newly synthesized dyes in organic solar cells. In general, all the synthesized PMIs show more or less optoelectronic competence which can be apprehended from the optical properties of the molecules discussed in earlier sections. However, the principal motive of choosing **2a** is its band alignment with the common acceptor, $PC_{61}BM$ (Phenyl-C_{61}-Butyric-Acid-Methyl-Ester). Here, **2a** has been used as donor or the absorber molecule. Recently, there are reports of using PMI based molecules as acceptor,[28] mainly because of high electronic conductivity due to conjugated backbones. On contrary, here, the molecules possess exciting optical absorption and seem suitable to be utilized as NIR absorbing or donor molecule. The device fabrication process and the device structure have been given in ESI.† In brief, the solar cell was composed of a transparent electrode, indium tin oxide (ITO) as the anode. A bare device (Fig. S17†) without any buffer layer has been prepared.

The current–voltage characteristics in dark and under solar simulator illumination and the power yield has been shown in Fig. 4. It can be easily noticed from the figure that there is a significant increase in current under illumination. Not only that, an open circuit voltage of 0.68 V is observed from this solar cell whereas the short-circuit current is 1.5 μA. Both the values validate the solar cell applicability of the **2a** molecule. The

Table 1 Summary of the optical and electrochemical properties of tetra-coupled PMI derivatives

Entry	λ_{abs}^{max} [a]/nm	λ_{Em}^{max} [a]/nm	SS[a]/cm^{-1}	E_{red} (1st)[b]/V	$E_{HOMO/LUMO}$ [b] eV	E_g [b]/eV
PMI	506	527	788	−1.20	−5.78/−3.50	2.28
1	523	560	1263	—[c]	—[c]	—[c]
2a	665	869	3531	−0.99	−5.54/−3.81	1.73
2b	614	659	1112	−0.94	−5.76/−3.86	1.90
2c	575	606	889	−0.93	−5.93/−3.87	2.06

[a] Measured in $CHCl_3$. [b] Measured in CH_2Cl_2. [c] Not determined due to poor solubility. All measurements were done at 298 K.

maximum power output from the solar cell device is 18 μW. The photo conversion efficiency of the solar cell is 0.002%. This value is low but it shows that the molecule is capable to convert light energy to electrical energy. Considering the bare device structure and primary functioning survey, the attainment of the **2a** molecule is substantial. When the results were compared with the PMI(Br)$_4$, which is the precursor of **2a**, we found that the precursor molecule was not capable of converting light energy to electrical energy.[18] PMI(Br)$_4$ showed enhancement in current under illumination and memory effect but was not essentially as suitable as **2a** for solar cell application. From the band diagram as shown in Fig. S16,† the high open circuit voltage of **2a** can be explained. The open circuit voltage of donor–acceptor solar cell depends on the HOMO–LUMO difference. The band diagram in Fig. S16† has been deduced from the HOMO, LUMO values **2a** as obtained from the DFT calculation. The difference between LUMO of $PC_{61}BM$ to HOMO of **2a** should be ~0.7 eV which is close to the V_{oc} obtained from solar cell prepared from a blend of **2a** and $PC_{61}BM$. Thus, from the above discussion, it could be realized that tetra-coupled PMI derivatives would be useful for the solar cell applications. The solar cell efficiency and performance can be improved if proper device configuration is followed which depends on the uniqueness of the dyes. Here, we performed a preliminary investigation using **2a** as solar absorber material; currently, we are involved in modifying the device configuration and tuning the other factors to improve the efficiency.

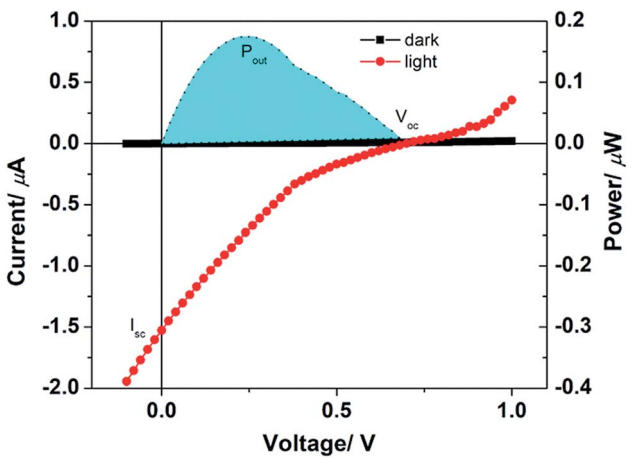

Fig. 4 Current–voltage and power yield characteristics of **2a** as donor molecule in dark and under solar simulator illumination.

In summary, we have successfully extended the π-conjugation along 1-, 6-, 9-, 10-positions of PMI using the optimized *tetra*-fold Sonogashira coupling protocol resulting in a series of NIR-absorbing PMI-based dyes possessing versatile functionalities. Extension of π-conjugation along *peri* position has a pronounced effect on the optoelectronic properties, which is evident from the remarkable bathochromic shifts in the absorption and emission spectra as compared to the unsubstituted PMI. Fascinatingly, NIR emitting PMI(NMe$_2$)$_4$ **2a** shows broad absorption and emission extending till 1200 nm and exhibits 204 nm Stokes shift which is a breakthrough in the field of PMI based derivatives. Also noteworthy is that PMI(NMe$_2$)$_4$ **2a** shows good photovoltaic property and further efforts are in progress. Finally, we anticipate that the ease of synthesis and tunable NIR properties of PMIs will allow entry into research on photovoltaic and solar cell applications.

Conflicts of interest

There are no conflicts to declare.

Acknowledgements

Council of Scientific & Industrial Research (Grant no: 02(0134)/17/EMR-II), India and IISER Bhopal and PSG Management are acknowledged for financial support.

Notes and references

1 B. A. Jones, A. Facchetti, M. R. Wasielewski and T. J. Marks, *Adv. Funct. Mater.*, 2008, **18**, 1329–1339.
2 G. H. Aryal, K. W. Hunter and L. Huang, *Org. Biomol. Chem.*, 2018, **16**, 7425–7429.
3 P. Brogdon, H. Cheema and J. H. Delcamp, *ChemSusChem*, 2018, **11**, 86–103.
4 S. Luo, E. Zhang, Y. Su, T. Cheng and C. Shi, *Biomaterials*, 2011, **32**, 7127–7138.
5 Y. Sang, Z. Zhao, M. Zhao, P. Hao, Y. Leng and H. Liu, *Adv. Mater.*, 2015, **27**, 363–369.
6 C. Hierlinger, H. V. Flint, D. B. Cordes, A. M. Z. Slawin, E. A. Gibson, D. Jacquemin, V. Guerchais and E. Zysman-Colman, *Polyhedron*, 2018, **140**, 109–115.
7 A. Laventure and G. C. Welch, *J. Mater. Chem. C*, 2018, **6**, 9060–9064.
8 S. Hao, Y. Shang, D. Li, H. Ågren, C. Yang and G. Chen, *Nanoscale*, 2017, **9**, 6711–6715.

9 T. Weil, T. Vosch, J. Hofkens, K. Peneva and K. Müllen, *Angew. Chem., Int. Ed.*, 2010, **49**, 9068–9093.
10 C. Li and H. Wonneberger, *Adv. Mater.*, 2012, **24**, 613–636.
11 K.-Y. Tomizaki, P. Thamyongkit, R. S. Loewe and J. S. Lindsey, *Tetrahedron*, 2003, **59**, 1191–1207.
12 R. S. Loewe, K.-y. Tomizaki, F. Chevalier and J. S. Lindsey, *J. Porphyrins Phthalocyanines*, 2002, **06**, 626–642.
13 J. Zhou, W. Zhang, X.-F. Jiang, C. Wang, X. Zhou, B. Xu, L. Liu, Z. Xie and Y. Ma, *J. Phys. Chem. Lett.*, 2018, **9**, 596–600.
14 C. Li and H. Wonneberger, *Adv. Mater.*, 2012, **24**, 613–636.
15 S. Mathew and H. Imahori, *J. Mater. Chem.*, 2011, **21**, 7166–7174.
16 C. Jung, B. K. Müller, D. C. Lamb, F. Nolde, K. Müllen and C. Bräuchle, *J. Am. Chem. Soc.*, 2006, **128**, 5283–5291.
17 A. Keerthi, Y. Liu, Q. Wang and S. Valiyaveettil, *Chem. - Eur. J.*, 2012, **18**, 11669–11676.
18 D. Sahoo, V. Sharma, R. Roy, N. Varghese, K. Mohanta and A. L. Koner, *Chem. Commun.*, 2019, **55**, 103–106.
19 K.-Y. Tomizaki, R. S. Loewe, C. Kirmaier, J. K. Schwartz, J. L. Retsek, D. F. Bocian, D. Holten and J. S. Lindsey, *J. Org. Chem.*, 2002, **67**, 6519–6534.
20 V. Sharma, D. Sahoo, F. Chandra and A. L. Koner, *ChemistrySelect*, 2017, **2**, 11747–11754.
21 K. Pal, V. Sharma and A. L. Koner, *Chem. Commun.*, 2017, **53**, 7909–7912.
22 C. Li, J. Schöneboom, Z. Liu, N. G. Pschirer, P. Erk, A. Herrmann and K. Müllen, *Chem. - Eur. J.*, 2009, **15**, 878–884.
23 V. Sharma, F. Chandra, D. Sahoo and A. L. Koner, *Eur. J. Org. Chem.*, 2017, **2017**, 6901–6905.
24 N. Kapuria, V. Sharma, P. Kumar and A. L. Koner, *J. Mater. Chem. C*, 2018, **6**, 11328–11335.
25 S. Mallick, K. Pal and A. L. Koner, *J. Colloid Interface Sci.*, 2016, **467**, 81–89.
26 K. Pal, I. Samanta, R. Gupta, D. Goswami and A. L. Koner, *Chem. Commun.*, 2018, **54**, 10590–10593.
27 Y. Hu, G. M. Paternò, X.-Y. Wang, X.-C. Wang, M. Guizzardi, Q. Chen, D. Schollmeyer, X.-Y. Cao, G. Cerullo, F. Scotognella, K. Müllen and A. Narita, *J. Am. Chem. Soc.*, 2019, **141**, 12797–12803.
28 Y. Zhang, X. Guo, B. Guo, W. Su, M. Zhang and Y. Li, *Adv. Funct. Mater.*, 2017, **27**, 1603892.